Journal of Integrative Neuroscience

J. Integr. Neurosci. **2026**; 25(10): 53689
https://doi.org/10.31083/JIN53689

Original Research

Electroacupuncture Inhibits Neuronal Ferroptosis in MCAO/R Model Mice by Regulating the GSK-3β/NRF2 Signaling Pathway

Wenxin Xia[1,†], Rui Zhao[1,†], Xiaoxiao Li[1], Chenchen Xu[1], Jianjian Dong[1,2], Shujie Li[1], Yun Xu[1], Yongsheng Han[1,2,3,*]

[1]Institute of Neurology, Anhui University of Chinese Medicine, 230061 Hefei, Anhui, China
[2]Center for Xin'an Medicine and Modernization of Traditional Chinese Medicine of IHM, Anhui University of Chinese Medicine, 230012 Hefei, Anhui, China
[3]Clinical College, Wannan Medical University, 241002 Wuhu, Anhui, China
*Correspondence: hyssp@126.com (Yongsheng Han)
[†]These authors contributed equally.

Academic Editor: Hahn Young Kim
Submitted: 8 May 2026 Revised: 24 August 2026 Accepted: 3 September 2026 Published: 13 October 2026

Abstract

Background: Neuronal ferroptosis following acute ischemic stroke (AIS) contributes to ischemic brain injury and is regulated by nuclear factor erythroid 2-related factor 2 (NRF2), a key regulator of antioxidant defense and iron homeostasis. Whether electroacupuncture (EA) suppresses neuronal ferroptosis by regulating NRF2 stability and nuclear translocation through upstream glycogen synthase kinase 3 beta (GSK-3β) remains unclear. We investigated whether EA inhibits neuronal ferroptosis and alleviates ischemic brain injury by modulating the GSK-3β/NRF2 axis. **Methods:** Middle cerebral artery occlusion/reperfusion (MCAO/R) models were established in C57BL/6 and conditional Nrf2-knockout mice. The GSK-3β inhibitor laduviglusib (CHIR-99021; CHIR), the ferroptosis inhibitor ferrostatin-1 (Fer-1), and conditional Nrf2 knockout were used to investigate the anti-ferroptotic mechanism of EA and the regulatory hierarchy between GSK-3β and NRF2. Reverse transcription quantitative polymerase chain reaction (RT-qPCR), western blotting, and immunofluorescence were used to examine the GSK-3β/NRF2 pathway and ferroptosis-related molecules. NRF2 nuclear localization, neuronal nuclei (NeuN) /acyl-CoA synthetase long-chain family member 4 (ACSL4) double immunofluorescence, and co-immunoprecipitation were used to assess NRF2 nuclear translocation, neuronal ferroptosis, and the GSK-3β–NRF2 interaction, respectively. **Results:** EA inhibited GSK-3β activity after MCAO/R, restored NRF2 protein expression, promoted nuclear accumulation, and upregulated NAD(P)H:quinone oxidoreductase 1 (NQO1). EA also downregulated ACSL4 and transferrin receptor 1 (TfR1), upregulated glutathione peroxidase 4 (GPX4) and solute carrier family 7 member 11 (SLC7A11), reduced NeuN/ACSL4-colocalized neurons, decreased ferrous iron (Fe^{2+}) and malondialdehyde (MDA) levels, and increased superoxide dismutase (SOD) activity, glutathione (GSH) content, and the GSH/oxidized glutathione (GSSG) ratio. CHIR and Fer-1 produced similar anti-ferroptotic effects, and co-immunoprecipitation confirmed GSK-3β–NRF2 interaction. Conditional Nrf2 knockout did not affect EA- or CHIR-mediated GSK-3β phosphorylation but markedly attenuated their effects on NQO1, SLC7A11, GPX4, and TfR1. EA also alleviated mitochondrial ultrastructural damage, reduced cerebral infarction and Fluoro-Jade B (FJB)-positive neurons, and improved neurological function and motor coordination in MCAO/R mice. **Conclusion:** These findings identify the GSK-3β/NRF2 axis as an important regulatory mechanism of regulating neuronal ferroptosis after MCAO/R and support EA as a potential therapeutic strategy for alleviating neuronal ferroptosis and cerebral ischemia-reperfusion injury through GSK-3β inhibition and NRF2 activation.

Keywords: electroacupuncture; ischemic stroke; reperfusion injury; glycogen synthase kinase 3 beta; NF-E2-related factor 2; ferroptosis

1. Introduction

Ischemic stroke (IS) results from compromised cerebral blood vessels and can lead to ischemia, hypoxia, necrosis, irreversible neuronal injury, and a series of molecular cascades, ultimately causing diverse neurological symptoms and sequelae; it remains a major cause of disability and death worldwide [1]. The principal pathological mechanisms of IS include energy depletion, excitotoxicity, free-radical generation, and oxidative stress [2]. At present, intravenous thrombolysis and mechanical thrombectomy are established reperfusion therapies for acute ischemic stroke, although their clinical application is constrained by therapeutic time windows and patient eligibility criteria [3].

Ferroptosis is an iron-dependent, non-apoptotic form of cell death that plays an important role in the pathogenesis of ischemic stroke. Its occurrence is associated with iron overload and the accumulation of lipid peroxides and reactive oxygen species (ROS). Excessive ROS accumulation can activate nuclear factor erythroid 2-related factor 2 (NRF2). NRF2 is a key regulator of cellular antioxidant responses and the expression of antioxidant- and ferroptosis-related genes. In particular, NRF2 transcriptionally regulates multiple key components of anti-ferroptotic pathways [4]; however, the upstream factors that regulate NRF2 remain incompletely understood.

Copyright: © 2026 The Author(s). Published by IMR Press.
This is an open access article under the CC BY 4.0 license.

Publisher's Note: IMR Press stays neutral with regard to jurisdictional claims in published maps and institutional affiliations.

Electroacupuncture (EA) combines traditional acupuncture with modern electrical stimulation [5]. Previous studies have shown that EA is commonly used in stroke treatment and may prevent stroke and promote post-stroke functional recovery by promoting angiogenesis [6] and reducing neuronal apoptosis [7] and by suppressing oxidative stress [8]. Our previous study showed that EA protects the neurovascular unit, reduces glycogen synthase kinase 3 beta (GSK-3β) expression, and improves neurological function in rats subjected to middle cerebral artery occlusion/reperfusion (MCAO/R) by modulating the Wnt/β-catenin pathway [9]. Other studies have suggested that EA alleviates ischemic brain injury in MCAO/R rats by inhibiting ferroptosis [10], potentially through NRF2 activation and increased protein expression of solute carrier family 7 member 11 (SLC7A11) and glutathione peroxidase 4 (GPX4) [11]. However, whether EA enhances NRF2 activity by inhibiting GSK-3β and thereby exerts anti-ferroptotic effects in neurons remains to be clarified.

GSK-3β is activated under hypoxic-ischemic conditions and contributes to neuronal death [12]. Studies have shown that GSK-3β inhibition in MCAO/R model animals promotes nuclear accumulation of NRF2, enabling its binding to antioxidant response elements (AREs) in the promoters of genes involved in the regulation of neuronal oxidative stress and thereby alleviating ischemic brain injury [13]. In addition, the GSK-3β/NRF2 signaling axis has been recognized as an important protective pathway against ferroptosis [14].

In this study, we systematically investigated the neuroprotective mechanisms of EA in a mouse model of MCAO/R-induced brain injury. The results showed that EA alleviated neuronal ferroptosis after acute ischemic stroke and exerted neuroprotective effects by modulating the upstream GSK-3β/NRF2 signaling pathway, inhibiting GSK-3β activity, and promoting NRF2 nuclear translocation.

2. Materials and Methods

2.1 Animals

Two types of experimental animals were used for different parts of this study.

For the first part of the study, 100 male C57BL/6 mice, specific pathogen-free (SPF) grade, weighing 20–22 g, were purchased from Hangzhou Ziyuan Experimental Animal Technology Co., Ltd. (laboratory animal production license No. SCXK [Zhejiang] 2019-0004). The animals were housed in a standard SPF animal facility at 22 ± 2 °C and 30%–50% relative humidity under a 12-h light/dark cycle, with six mice per cage and free access to standard laboratory chow and water. Before the experiments, the mice were acclimatized under these conditions.

For the second part of the study, homozygous $Nrf2^{f/f}$ mice and Nestin-Cre mice were purchased from Shanghai Model Organisms Center, Inc. Male and female mice were paired according to the established breeding scheme. After birth, tail tissue was collected from the offspring, genomic deoxyribonucleic acid (DNA) was extracted using a mouse-tail genomic DNA extraction kit, and genotyping was performed by polymerase chain reaction (PCR). Male $Nrf2^{f/f}$ and $Nrf2^{f/f}$;Nestin-Cre mice required for the experiments were selected based on agarose gel electrophoresis of the PCR products; representative gel electrophoresis results are shown in **Supplementary Fig. 1**. Experimental mice were 4–5 months old and weighed 25–30 g. All animals were housed in a conventional laboratory animal facility at 24–26 °C and 50%–60% relative humidity under a 12-h light/dark cycle, with free access to food and water.

2.2 Grouping and Treatment

2.2.1 Experimental Design in C57BL/6 Mice

The experimental workflow and timeline are shown in Fig. 1C. To evaluate the effects of EA on MCAO/R-induced cerebral ischemia-reperfusion injury and the role of GSK-3β, 112 male C57BL/6 mice were used in the main experiment, of which 100 were ultimately included. Forty sham-operated mice were randomly assigned to the Sham and Sham + CHIR groups (n = 20 per group). The remaining mice underwent MCAO/R modeling, and those meeting the inclusion criteria were randomly assigned to the MCAO/R, MCAO/R + EA, and MCAO/R + CHIR groups (n = 20 per group). Animal inclusion, exclusion, and mortality are detailed in **Supplementary Table 1**.

The MCAO/R model was established using a modified Zea Longa intraluminal filament method. Mice in the Sham group underwent the same surgical procedures without filament insertion. Mice in the MCAO/R + EA group received EA after successful model establishment, whereas mice in the Sham + CHIR and MCAO/R + CHIR groups received the GSK-3β inhibitor laduviglusib (CHIR-99021; hereafter referred to as CHIR) hydrochloride. Detailed modeling procedures, drug doses, and EA parameters are described in the corresponding experimental sections.

To further verify the role of ferroptosis in MCAO/R injury, an additional MCAO/R + ferrostatin-1 (Fer-1) group was established. Eight mice were used in this experiment, of which five were ultimately included; detailed inclusion and exclusion information is provided in **Supplementary Table 1**. Ferrostatin-1 (Fer-1; S7243, Selleck Chemicals, Houston, TX, USA) was administered intraperitoneally at 10 mg/kg at 24 h and 2 h before MCAO/R surgery.

2.2.2 Experimental Design in Conditional Nrf2-Knockout Mice

To verify the role of NRF2 in the effects of EA on MCAO/R-induced brain injury and its regulatory relationship with GSK-3β, a total of 55 male $Nrf2^{f/f}$ and $Nrf2^{f/f}$;Nestin-Cre ($Nrf2^{f/N}$) mice were used, of which 40 were ultimately included and allocated to eight groups (n = 5 per group): $Nrf2^{f/f}$, $Nrf2^{f/f}$ + M/R, $Nrf2^{f/f}$ + M/R + EA, $Nrf2^{f/f}$ + M/R + CHIR, $Nrf2^{f/N}$, $Nrf2^{f/N}$ + M/R, $Nrf2^{f/N}$ +

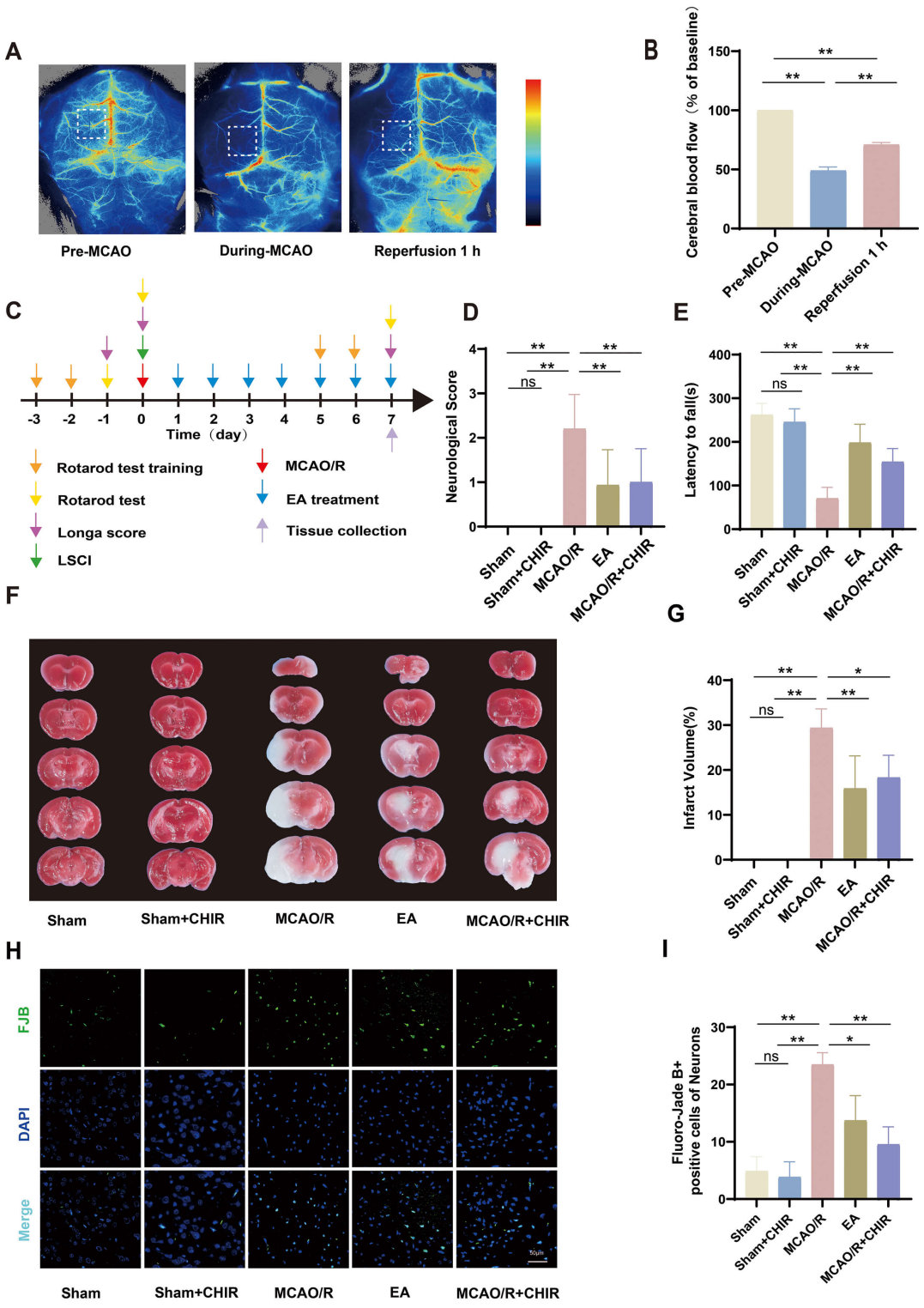


Fig. 1. EA improves neurological function and reduces ischemic brain injury after MCAO/R. (A) Laser speckle images of cerebral blood flow before MCA occlusion, during occlusion, and 1 h after reperfusion; dashed boxes indicate the ipsilateral region used for analysis. (B) Cerebral blood flow quantification (n = 3). (C) Experimental timeline. (D) Longa neurological deficit score (n = 15). (E) Rotarod latency to fall (n = 15). (F,G) TTC staining and infarct-volume quantification (n = 4). (H,I) FJB staining and quantification of FJB-positive neurons (n = 3); nuclei were counterstained with DAPI. Scale bar = 50 μm. Values are mean ± SD; ns, not significant; *$p < 0.05$, **$p < 0.01$. EA, electroacupuncture; MCAO/R, middle cerebral artery occlusion/reperfusion; MCA, middle cerebral artery; TTC, 2,3,5-Triphenyltetrazolium Chloride; FJB, Fluoro-Jade B; DAPI, 4′,6-diamidino-2-phenylindole; SD, standard deviation.

M/R + EA, and $Nrf2^{f/N}$ + M/R + CHIR. In these group labels, M/R denotes MCAO/R.

For the conditional Nrf2-knockout experiment involving EA, 38 mice were used and 30 were ultimately included, comprising non-MCAO/R control, M/R, and M/R + EA groups for each genotype (n = 5 per group). On this basis, an additional 17 mice were used for the CHIR-99021 intervention experiment, with 10 additional mice ultimately included in the $Nrf2^{f/f}$ + M/R + CHIR and $Nrf2^{f/N}$ + M/R + CHIR groups (n = 5 per group). The M/R groups for both genotypes used the same animals and samples described above.

MCAO/R modeling, model inclusion criteria, EA treatment, and CHIR-99021 intervention were performed as described in the corresponding sections above. Animal use, inclusion, and exclusion for all groups are detailed in **Supplementary Table 1**.

2.3 MCAO/R Mouse Model Construction

A mouse middle cerebral artery occlusion/reperfusion (MCAO/R) model was established using a modified intraluminal filament method, with the territory supplied by the left middle cerebral artery (MCA) designated as the ischemic side. Mice were anesthetized by intraperitoneal injection of sodium pentobarbital (50 mg/kg), and body temperature was maintained at 37 ± 0.5 °C during surgery. After exposure of the left common carotid artery (CCA), external carotid artery (ECA), and internal carotid artery (ICA), an incision was made near the CCA bifurcation. A 0.2-mm-diameter filament (1220-A5, Beijing Xinong Technology Co., Ltd.) was inserted through the CCA into the ICA and advanced approximately 9.0 ± 0.5 mm to occlude MCA blood flow. After 60 min of ischemia, the filament was slowly withdrawn to restore perfusion. After recovery from anesthesia, neurological function was assessed using the Zea Longa scoring system [15]. Mice with scores of 1–3 were considered to have successful MCAO/R induction and were included in subsequent experiments. Animals that did not meet the predefined inclusion criteria were excluded, and additional modeling was performed to maintain the planned sample size for each group.

2.4 Electroacupuncture Treatment and Drug Dosage and Administration

After successful modeling, the mice were anesthetized with sodium pentobarbital (50 mg/kg). According to the Chinese Association of Acupuncture-Moxibustion standard, Nomenclature and Location of Acupuncture Points Commonly Used in Laboratory Animals—Part 3: Mice, the principal acupoints of the Xingnao Kaiqiao acupuncture method were selected: Baihui (GV20), Shuigou (GV26), bilateral Neiguan (PC6), and bilateral Sanyinjiao (SP6) [16]. Disposable acupuncture needles were inserted perpendicularly to a depth of approximately 1 mm at PC6, obliquely upward to approximately 1 mm at GV26, perpendicularly to approximately 2 mm at SP6, and obliquely forward to approximately 2 mm at GV20. During needle retention, bilateral PC6 and SP6 were connected to an electroacupuncture apparatus using a dense-disperse wave at 2/100 Hz and 2–4 V, with the stimulation intensity gradually adjusted until slight local muscle twitching was observed at the needling sites. EA parameters were based on Zhu et al. [11]. EA was initiated on day 1 after MCAO/R and administered once daily for 7 consecutive days. All procedures were performed by the same trained experimenter.

Mice in the Sham + CHIR, MCAO/R + CHIR, $Nrf2^{f/f}$ + M/R + CHIR, and $Nrf2^{f/N}$ + M/R + CHIR groups received intracerebroventricular injections of the GSK-3β inhibitor laduviglusib (CHIR-99021) hydrochloride ((Cat. No. S2924; batch No. S292407; Selleck Chemicals, Shanghai, China)) at 8 μg/kg on day 3 before modeling and 1 h before modeling. Injections were performed using a stereotaxic apparatus. Based on Mouse Brain in Stereotaxic Coordinates [17], the lateral ventricle coordinates were 0.5 mm posterior to bregma, 1.0 mm left of the midline, and 1.8 mm below the dura. A 10-μL microsyringe was used for slow injection over 10 min, and the needle was left in place for 8 min after injection to minimize leakage.

2.5 Rotarod Test

Motor coordination was assessed using the rotarod test (n = 15/group). After 2 days of acclimatization training, formal testing was conducted on day 3, with the rotation speed gradually increased from 5 to 40 rpm. Each mouse underwent three trials (maximum 5 min/trial; interval ≥30 min). The latency to fall was recorded, and the mean of the three trials was used for analysis.

2.6 Laser Speckle Contrast Imaging of Cerebral Blood Flow

Cerebral blood flow (CBF) was monitored in real time using a laser speckle contrast imaging (LSCI) system. Mice were induced with 4% isoflurane anesthesia and maintained with 2% isoflurane (O_2 flow rate, 0.8 L/min) while prone on a temperature-controlled stereotaxic plate (37.0 ± 0.5 °C). The skull was exposed and kept moist with saline. CBF images were acquired in temporal-filtering mode (250 frames, 5 s/frame). The left MCA territory was selected as the region of interest (ROI) for blood-flow analysis. Results were expressed in arbitrary units (AU) and displayed using a 12-color pseudocolor map.

2.7 2,3,5-Triphenyltetrazolium Chloride (TTC) Staining

On day 7 after MCAO/R, four mice were randomly selected from each group and deeply anesthetized by intraperitoneal injection of sodium pentobarbital (50 mg/kg). After adequate depth of anesthesia was confirmed, the mice were perfused with saline and euthanized by decapitation for brain collection. Brain tissue was frozen at −20 °C for approximately 20 min and then cut into five 2-mm-thick coronal slices. The slices were incubated in 2% TTC solu-

tion at 37 °C in the dark for 30 min and turned every 10 min. After staining, the slices were fixed in 4% paraformaldehyde for 24 h and photographed. Normal brain tissue appeared red, whereas infarcted areas appeared white. Quantitative analysis was performed using ImageJ software by an independent investigator blinded to animal grouping and interventions. The percentage cerebral infarct volume was calculated as follows: cerebral infarct volume (%) = total infarcted tissue volume/total brain tissue volume × 100%.

2.8 Fluoro-Jade B (FJB) Staining for Assessment of Neuronal Injury

Paraffin-embedded brain sections were routinely deparaffinized and rehydrated. A Fluoro-Jade B (FJB) working solution was prepared at 1:100 in 0.1% glacial acetic acid, and sections were incubated at room temperature in the dark for 30 min. Sections were counterstained with 4′,6-diamidino-2-phenylindole (DAPI) for 8 min and washed. After thorough drying, the sections were cleared with xylene and mounted with neutral resin. Quantitative analysis was performed using ImageJ software (version 1.54p; National Institutes of Health, Bethesda, MD, USA) by an independent investigator who was not involved in animal randomization, group allocation, or administration of the interventions and remained blinded to group assignment during the analysis.

2.9 Transmission Electron Microscopy (TEM)

On day 7 after modeling, five mice were randomly selected from each group, anesthetized, and transcardially perfused with saline. The brains were rapidly removed, and ipsilateral ischemic cortical tissue was dissected. The tissue was cut into approximately 1-mm^3 pieces, immediately placed in electron microscopy fixative, and fixed at 4 °C. Samples were then post-fixed with 1% osmium tetroxide for 2 h, dehydrated through a graded ethanol series, embedded in epoxy resin, and polymerized at 60 °C for 48 h. Ultrathin sections (50–80 nm) were prepared using an ultramicrotome, stained, and examined and imaged by transmission electron microscopy.

2.10 Reverse Transcription-Quantitative Polymerase Chain Reaction (RT-qPCR)

Brain tissue (10 mg) was homogenized using an electric homogenizer at 60 Hz for 45 s. Procedures were performed according to the manufacturers' instructions for the PCR kits (AC0202 and AG0304, Sparkjade, Jinan, China). Gapdh and β-actin were used as reference genes, and relative target-gene expression was calculated using the $2^{-\Delta\Delta Ct}$ method. Primer sequences are provided in **Supplementary Table 2**.

2.11 Co-Immunoprecipitation (Co-IP)

Brain tissue (20 mg) was homogenized using an electric homogenizer at 60 Hz for 45 s. According to the kit instructions (P2179, Beyotime, Shanghai, China), Protein A+G magnetic beads were used for co-immunoprecipitation (Co-IP) of GSK-3β and NRF2, and the recovered proteins were subsequently analyzed by western blotting.

2.12 Western Blotting

Brain tissue (50 mg) was homogenized in radioimmunoprecipitation assay (RIPA) lysis buffer containing phenylmethylsulfonyl fluoride (PMSF), and total protein was extracted. Equal amounts of protein were separated by 8%–12% sodium dodecyl sulfate-polyacrylamide gel electrophoresis (SDS-PAGE) and transferred to 0.2-μm nitrocellulose (NC) membranes. After blocking, membranes were incubated overnight at 4 °C with the following primary antibodies: NRF2 (1:1000, Cat. No. GB115673, Servicebio, Wuhan, Hubei, China; Cat. No. 380773, Zenbio, Chengdu, Sichuan, China), p-GSK-3β (1:1000, Cat. No. 5558, Cell Signaling Technology, Danvers, MA, USA), GSK-3β (1:1000, Cat. No. 9315, Cell Signaling Technology, Danvers, MA, USA), ACSL4 (1:1000, Cat. No. 384265, Zenbio, Chengdu, Sichuan, China; Cat. No. A20414, ABclonal, Wuhan, Hubei, China), GPX4 (1:2000, Cat. No. 381958, Zenbio, Chengdu, Sichuan, China), SLC7A11 (1:1000, Cat. No. R382036, Zenbio, Chengdu, Sichuan, China), NQO1 (1:1000, Cat. No. ab34173, Abcam, Cambridge, UK), TfR1 (1:1000, Cat. No. A5865SP, ABclonal, Wuhan, Hubei, China), β-tubulin (1:3000, Cat. No. 380628, Zenbio, Chengdu, Sichuan, China), GAPDH (1:3500, Cat. No. GB11002, Servicebio, Wuhan, Hubei, China), and histone H3 (1:1000, Cat. No. 381432, Zenbio, Chengdu, Sichuan, China).After washing, membranes were incubated with the corresponding secondary antibodies (1:10,000) for 1.5 h at room temperature. Signals were developed using enhanced chemiluminescence (ECL), and band intensities were quantified using ImageJ software (version 1.54p; National Institutes of Health, Bethesda, MD, USA).

2.13 Immunofluorescence Staining

Paraffin-embedded mouse brain sections (4 μm) were deparaffinized, hydrated, and subjected to antigen retrieval, followed by blocking with calf serum at 37 °C for 1 h. Sections were incubated overnight at 4 °C with primary antibodies against NRF2, ACSL4, and NeuN (1:100), washed, and then incubated with the corresponding Alexa Fluor 488- and Alexa Fluor 594-conjugated secondary antibodies (1:500) for 1 h at room temperature in the dark. Nuclei were counterstained with DAPI, and sections were mounted and imaged using a Nikon Eclipse C1 fluorescence microscope. Quantitative analysis was performed using CaseViewer software (version 2.4; 3DHISTECH Ltd., Budapest, Hungary).

2.14 Measurement of Fe^{2+} and Oxidative Stress-Related Indicators

The levels of Fe^{2+}, superoxide dismutase (SOD), malondialdehyde (MDA), reduced glutathione (GSH), and oxidized glutathione (GSSG) in the ischemic cortex were measured using commercial assay kits (Beijing Solarbio Science & Technology Co., Ltd., Beijing, China) according to the manufacturer's instructions. Briefly, cerebral cortex tissues were homogenized and centrifuged, and the supernatants were collected for subsequent analysis. Fe^{2+} content was measured at 593 nm, SOD activity was determined at 560 nm, MDA content was detected at 532 nm and 600 nm, and GSH and GSSG levels were measured at 412 nm using a microplate reader. The GSH/GSSG ratio was calculated based on the measured GSH and GSSG concentrations.

2.15 Statistical Analysis

Statistical analyses were performed using SPSS 23.0 (IBM, Armonk, NY, USA). Data are presented as mean ± standard deviation (SD). As appropriate, comparisons between two groups were performed using *t* tests, whereas comparisons among three or more groups were performed using one-way analysis of variance (ANOVA) followed by Tukey's post hoc test. For repeated measurements, one-way repeated-measures ANOVA followed by Tukey's multiple comparisons test was performed. $p < 0.05$ was considered statistically significant, and $p < 0.01$ was considered highly statistically significant. Data visualization was performed using GraphPad Prism v.9.0.0 (GraphPad Software, San Diego, CA, USA).

3. Results

3.1 Electroacupuncture Improves Neurological Function and Reduces Cerebral Infarct Volume and Neuronal Injury in MCAO/R Mice

LSCI showed that CBF in the ischemic region decreased significantly after MCA occlusion compared with the pre-modeling level and partially recovered 1 h after reperfusion but remained below the baseline level (all $p < 0.01$, Fig. 1A,B), indicating successful establishment of the MCAO/R model. The experimental workflow and assessment time points are shown in Fig. 1C.

Compared with the Sham group, the MCAO/R group had higher Longa scores, shorter rotarod fall latencies, and significantly greater cerebral infarct volumes and numbers of FJB-positive neurons (all $p < 0.01$, Fig. 1D–I). These abnormalities were significantly improved by EA or CHIR treatment ($p < 0.05$ or $p < 0.01$), whereas no significant differences were observed between the Sham + CHIR and Sham groups ($p > 0.05$, Fig. 1D–I).

Collectively, both EA and GSK-3β inhibition improved neurological deficits and motor coordination after MCAO/R and reduced cerebral infarction and neuronal injury. Their similar neuroprotective effects suggest that GSK-3β may participate in the regulation of cerebral ischemia-reperfusion injury by EA.

3.2 Electroacupuncture Attenuates Mitochondrial Injury, Abnormal Fe^{2+} Accumulation, and Ferroptosis-Related Oxidative Damage in MCAO/R Mice

After establishing the neuroprotective effect of EA against MCAO/R-induced brain injury, we further evaluated its effects on ferroptosis-related changes. Transmission electron microscopy showed mitochondrial shrinkage or swelling, abnormal membrane structure, and disorganized, reduced, or absent cristae after MCAO/R (Fig. 2A), accompanied by a significant increase in the proportion of damaged mitochondria ($p < 0.01$, Fig. 2B). Both EA and CHIR markedly improved mitochondrial ultrastructure and reduced the proportion of damaged mitochondria ($p < 0.05$ or $p < 0.01$).

Compared with the Sham group, the MCAO/R group showed significantly increased brain Fe^{2+} and malondialdehyde (MDA) levels and significantly decreased superoxide dismutase (SOD) activity, glutathione (GSH) content, and GSH/oxidized glutathione (GSSG) ratio (all $p < 0.01$, Fig. 2C–G). Both EA and CHIR significantly reversed these changes (all $p < 0.01$).

These results indicate that EA attenuates MCAO/R-induced mitochondrial injury, iron accumulation, and oxidative lipid damage. CHIR produced similar effects, suggesting that GSK-3β may participate in the regulation of ferroptosis-related injury after MCAO/R by EA.

3.3 Electroacupuncture Ameliorates Abnormal Expression of Ferroptosis-Related Molecules in MCAO/R Mice

The preceding results showed that EA attenuated MCAO/R-induced mitochondrial injury, Fe^{2+} accumulation, and redox imbalance. To further evaluate the regulation of ferroptosis by EA, we measured the expression of ferroptosis-related molecules and used the ferroptosis inhibitor Fer-1 as a pharmacological reference.

RT-qPCR showed that MCAO/R significantly upregulated ACSL4 and TfR1 mRNA expression and downregulated GPX4 mRNA expression, whereas EA, CHIR, and Fer-1 significantly reversed these changes (all $p < 0.01$, Fig. 3A–C). Western blotting further showed that MCAO/R significantly increased ACSL4 and TfR1 protein expression and decreased GPX4 and SLC7A11 expression; EA, CHIR, and Fer-1 reversed these changes to varying degrees ($p < 0.05$ or $p < 0.01$, Fig. 3D–H).

These results indicate that EA significantly ameliorates MCAO/R-induced abnormalities in ferroptosis-related molecules, with an effect pattern similar to that of Fer-1. The GSK-3β inhibitor CHIR produced consistent effects, suggesting that GSK-3β may participate in the regulation of ferroptosis by EA. On this basis, the GSK-3β/NRF2 signaling pathway was further examined to investigate the potential molecular mechanism by which EA inhibits ferroptosis.

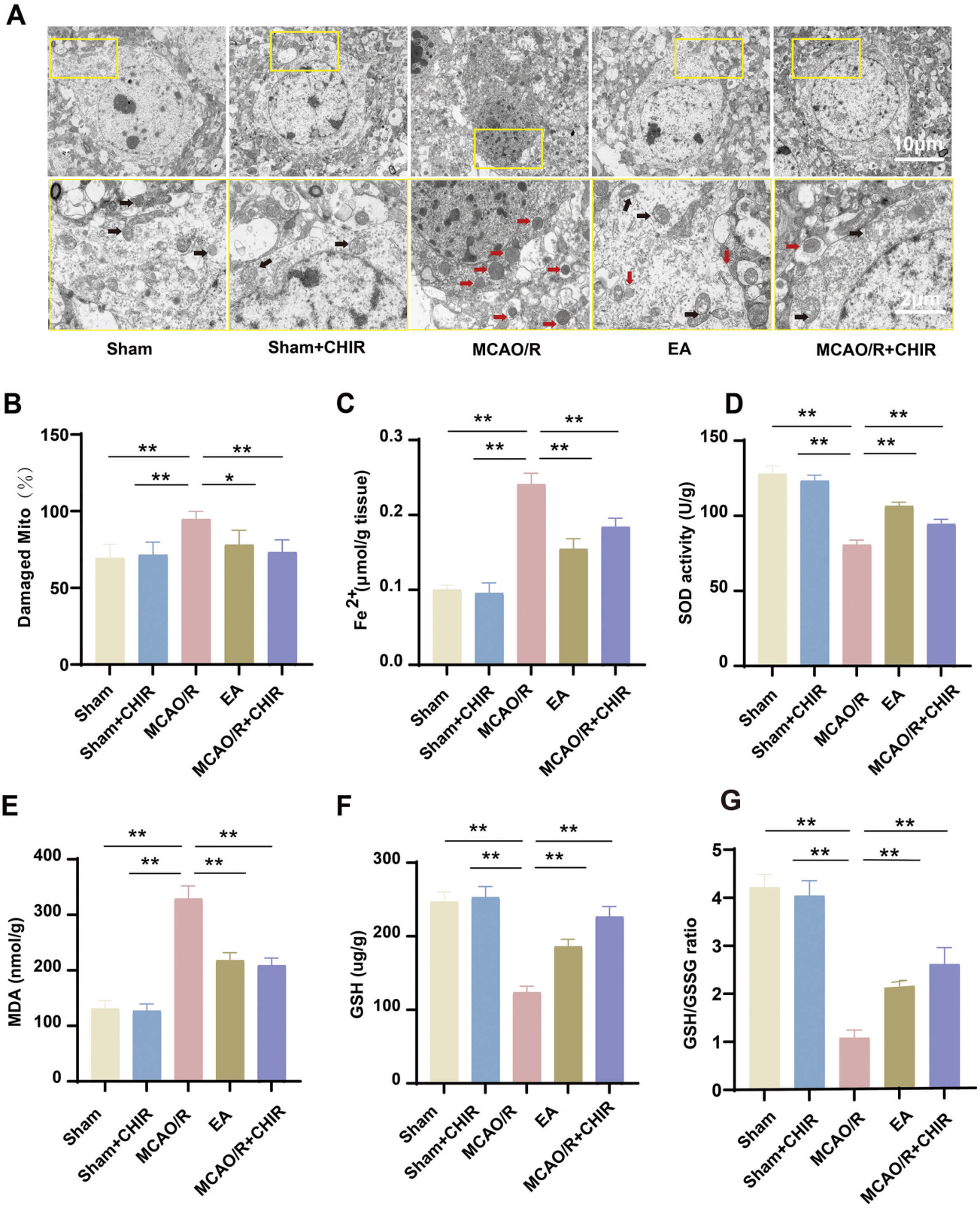


Fig. 2. EA attenuates mitochondrial damage, ferrous iron (Fe^{2+}) accumulation, and oxidative injury after MCAO/R. (A) Transmission electron microscopy of brain tissue (n = 5); lower panels are magnified views of the boxed regions, and black and red arrows indicate normal and damaged mitochondria, respectively. Scale bars = 10 μm (upper panels) and 2 μm (lower magnified panels). (B) Damaged mitochondria (n = 5). (C) Fe^{2+} content (n = 5). (D) SOD activity (n = 5). (E) MDA content (n = 5). (F) GSH content (n = 5). (G) GSH/GSSG ratio (n = 5). Values are mean ± SD; *$p < 0.05$, **$p < 0.01$. SOD, superoxide dismutase; MDA, malondialdehyde; GSH, glutathione; GSSG, GSH/oxidized glutathione.

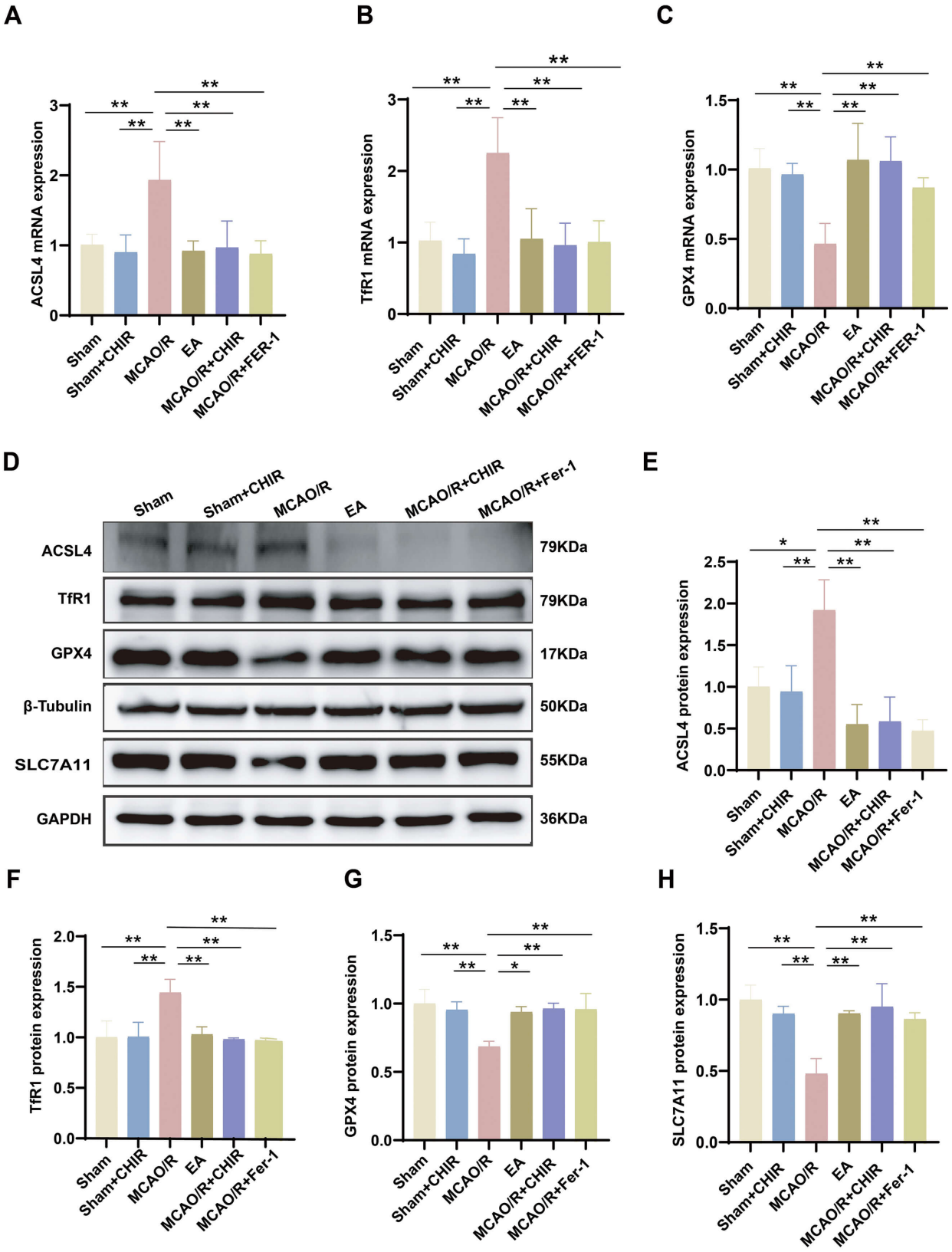


Fig. 3. EA normalizes ferroptosis-related molecular changes after MCAO/R. (A–C) RT-qPCR analysis of ACSL4 (A), TfR1 (B), and GPX4 (C) mRNA expression (n = 5). (D) Representative western blots of ACSL4, TfR1, GPX4, and SLC7A11. (E–H) Densitometric quantification of ACSL4 (E), TfR1 (F), GPX4 (G), and SLC7A11 (H) protein expression (n = 3). Values are mean ± SD; *$p < 0.05$, **$p < 0.01$. RT-qPCR, reverse transcription quantitative polymerase chain reaction; GPX4, glutathione peroxidase 4; SLC7A11, solute carrier family 7 member 11; ACSL4, acyl-CoA synthetase long-chain family member 4; TfR1, transferrin receptor 1.

3.4 Electroacupuncture Inhibits MCAO/R-Induced Ferroptosis by Modulating the GSK-3β/NRF2 Signaling Pathway

3.4.1 Electroacupuncture Inhibits GSK-3β Activity and Promotes NRF2 Nuclear Translocation

The preceding results showed that EA ameliorated MCAO/R-induced redox imbalance and ferroptosis-related changes. To further investigate the underlying mechanism, we examined the GSK-3β/NRF2 signaling pathway using the GSK-3β inhibitor CHIR as a pharmacological reference.

After MCAO/R, Nrf2 mRNA expression was significantly increased ($p < 0.05$, Fig. 4A), whereas total NRF2 protein levels were markedly decreased ($p < 0.01$, Fig. 4C,E). EA further increased Nrf2 mRNA expression ($p < 0.01$, Fig. 4A) and significantly restored total NRF2 protein expression ($p < 0.01$, Fig. 4C,E). Immunofluorescence showed greater nuclear NRF2 fluorescence in the MCAO/R group than in the Sham group; nuclear NRF2 was further significantly increased after EA and CHIR treatment ($p < 0.01$ or $p < 0.05$, Fig. 4H,I).Western blotting of nuclear extracts yielded consistent results, with EA significantly increasing nuclear NRF2 expression ($p < 0.05$, Fig. 4D,E). In parallel, expression of the NRF2 downstream antioxidant protein NQO1 was restored (Fig. 4E and **Supplementary Fig. 2**), indicating that EA promotes NRF2 accumulation and nuclear translocation and enhances the downstream antioxidant response.

Further analysis showed that GSK-3β mRNA expression increased after MCAO/R ($p < 0.01$, Fig. 4B), whereas the p-GSK-3β/GSK-3β ratio decreased ($p < 0.01$, Fig. 4E,F). Both EA and CHIR significantly reversed these changes ($p < 0.01$, Fig. 4B,E,F). In addition, Co-IP demonstrated a protein interaction between GSK-3β and NRF2 (Fig. 4G). Together with the CHIR-induced increases in NRF2 protein expression and nuclear accumulation, these findings suggest that GSK-3β may participate in the regulation of NRF2 stability and nuclear translocation.

Collectively, EA inhibited GSK-3β activity after MCAO/R, restored NRF2 protein expression, promoted NRF2 nuclear translocation, and increased downstream NQO1 expression. These findings suggest that EA may enhance antioxidant defense by modulating the GSK-3β/NRF2 signaling axis, thereby suppressing MCAO/R-related ferroptosis.

3.4.2 Electroacupuncture Modulates ACSL4/GPX4 Expression and Attenuates MCAO/R-Induced Neuronal Ferroptosis

Based on the changes in GSK-3β/NRF2 signaling and antioxidant effects described above, we further evaluated the regulation of MCAO/R-induced ferroptosis by EA at the neuronal level. Western blotting showed that, compared with the Sham group, the MCAO/R group had significantly increased ACSL4 expression and significantly decreased GPX4 expression ($p < 0.01$, Fig. 5A–C). EA significantly reversed these changes ($p < 0.05$ for ACSL4 and $p < 0.01$ for GPX4, Fig. 5A–C), and CHIR produced similar effects ($p < 0.01$, Fig. 5A–C).

NeuN/ACSL4 double immunofluorescence further showed that MCAO/R significantly increased neuronal ACSL4 expression and the number of NeuN/ACSL4-colocalized positive cells, whereas both EA and CHIR significantly suppressed these changes (both $p < 0.01$, Fig. 5D,E). These results further demonstrate that EA attenuates MCAO/R-induced neuronal ferroptosis-associated changes and that GSK-3β inhibition produces similar effects, consistent with the preceding findings on GSK-3β/NRF2 signaling.

3.5 Conditional Nrf2 Knockout Demonstrates the Key Role of Nrf2 in Electroacupuncture-Mediated Inhibition of MCAO/R-Induced Ferroptosis

The preceding results showed that EA modulated GSK-3β/NRF2 signaling and attenuated MCAO/R-induced neuronal ferroptosis. To further determine the role of NRF2 in this process, conditional Nrf2-knockout mice were used.

In $Nrf2^{f/f}$ mice, MCAO/R increased Nrf2 mRNA expression but decreased NRF2 protein expression, and EA further increased Nrf2 mRNA expression and restored NRF2 protein levels ($p < 0.05$ or $p < 0.01$, Fig. 6A,D,E). In $Nrf2^{f/N}$ mice, NRF2 protein remained at a low level and was not significantly restored by EA ($p > 0.05$, Fig. 6E). No significant differences in GSK-3β mRNA expression were observed among the groups ($p > 0.05$, Fig. 6B). Notably, the MCAO/R-induced decrease in the p-GSK-3β/GSK-3β ratio and its EA-mediated restoration persisted in $Nrf2^{f/N}$ mice ($p < 0.05$ or $p < 0.01$, Fig. 6D,F), indicating that Nrf2 deficiency does not affect EA-mediated regulation of GSK-3β phosphorylation.

In contrast, Nrf2 deficiency markedly attenuated the effects of EA on downstream molecules. In $Nrf2^{f/f}$ mice, EA reversed MCAO/R-induced downregulation of NQO1, SLC7A11, and GPX4 and upregulation of TfR1; these effects were markedly weakened in $Nrf2^{f/N}$ mice ($p < 0.05$ or $p < 0.01$, Fig. 6C,G–N).

Collectively, Nrf2 deficiency did not affect EA-mediated regulation of upstream GSK-3β phosphorylation but markedly attenuated its beneficial effects on NQO1 and ferroptosis-related molecules, supporting Nrf2 as a key downstream mediator of the antioxidant and anti-ferroptotic effects of EA regulated by GSK-3β.

3.6 Conditional Nrf2 Knockout Attenuates the Beneficial Effects of GSK-3β Inhibition on MCAO/R-Induced Ferroptosis

The preceding results showed that conditional Nrf2 knockout attenuated the effects of EA on abnormal expression of ferroptosis-related molecules after MCAO/R. To further clarify the regulatory hierarchy between GSK-3β and NRF2, the GSK-3β inhibitor CHIR was used.

RT-qPCR showed no significant differences in GSK-3β mRNA expression among the groups ($p > 0.05$, Fig. 7A).

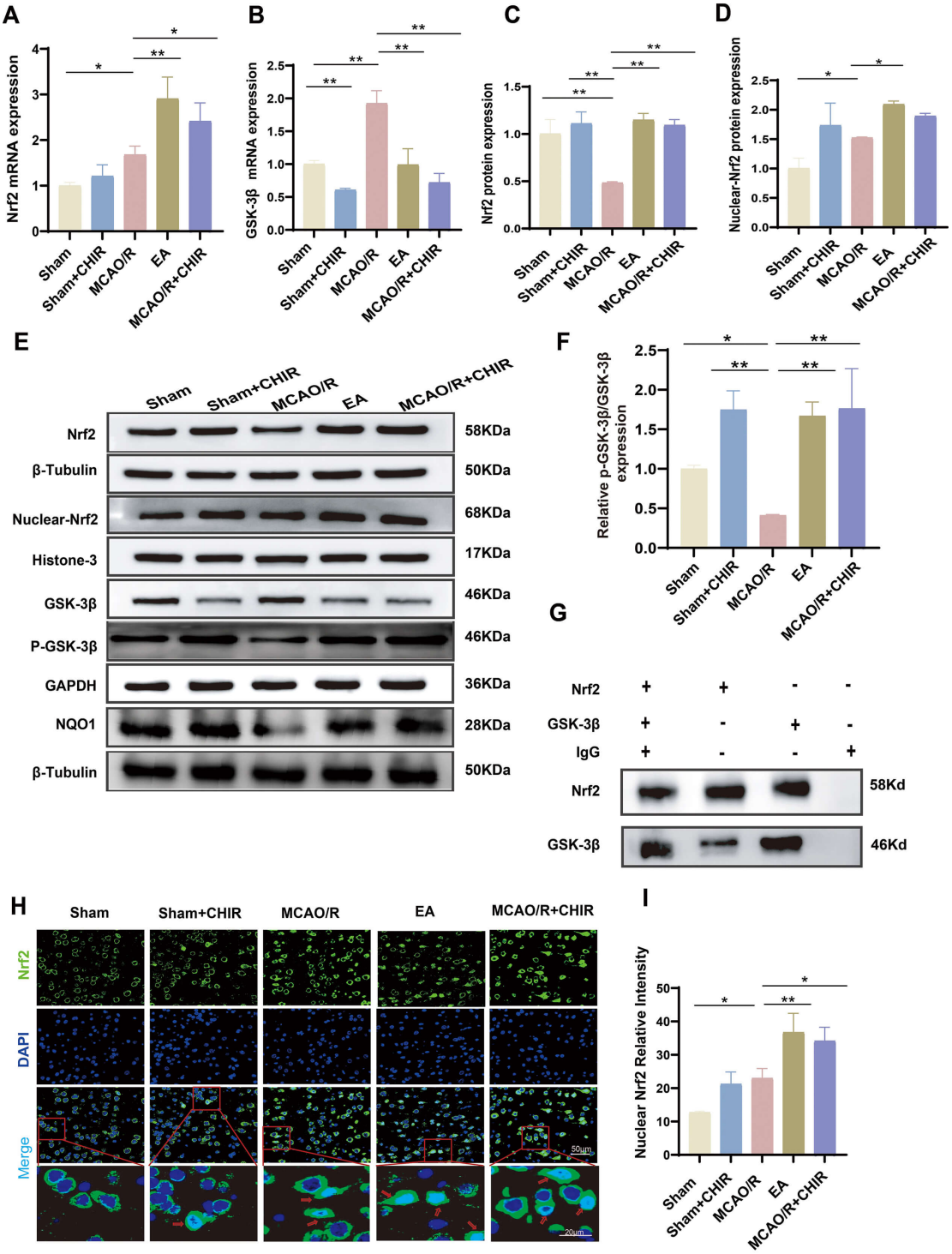


Fig. 4. EA inhibits GSK-3β activity and promotes NRF2 accumulation and nuclear translocation. (A,B) RT-qPCR analysis of Nrf2 (A) and GSK-3β (B) mRNA expression in the ipsilateral ischemic cortex (n = 5). (C,D) Quantification of total and nuclear NRF2 protein, respectively (n = 3). (E) Representative western blots of total NRF2, nuclear NRF2, GSK-3β, p-GSK-3β, and NQO1; NQO1 quantification is shown in **Supplementary Fig. 2**. (F) p-GSK-3β/GSK-3β ratio (n = 3). (G) Co-immunoprecipitation of GSK-3β and NRF2. (H) NRF2 immunofluorescence in the ipsilateral ischemic cortex; NRF2 is green, nuclei are blue, and arrows indicate nuclear NRF2. Scale bars = 50 μm (merged images) and 20 μm(magnified images). (I) Relative nuclear NRF2 fluorescence intensity (n = 3). Values are mean ± SD; *$p < 0.05$, **$p < 0.01$. GSK-3β, glycogen synthase kinase 3 beta; NRF2, nuclear factor erythroid 2-related factor 2; NQO1, NAD(P)H:quinone oxidoreductase 1.

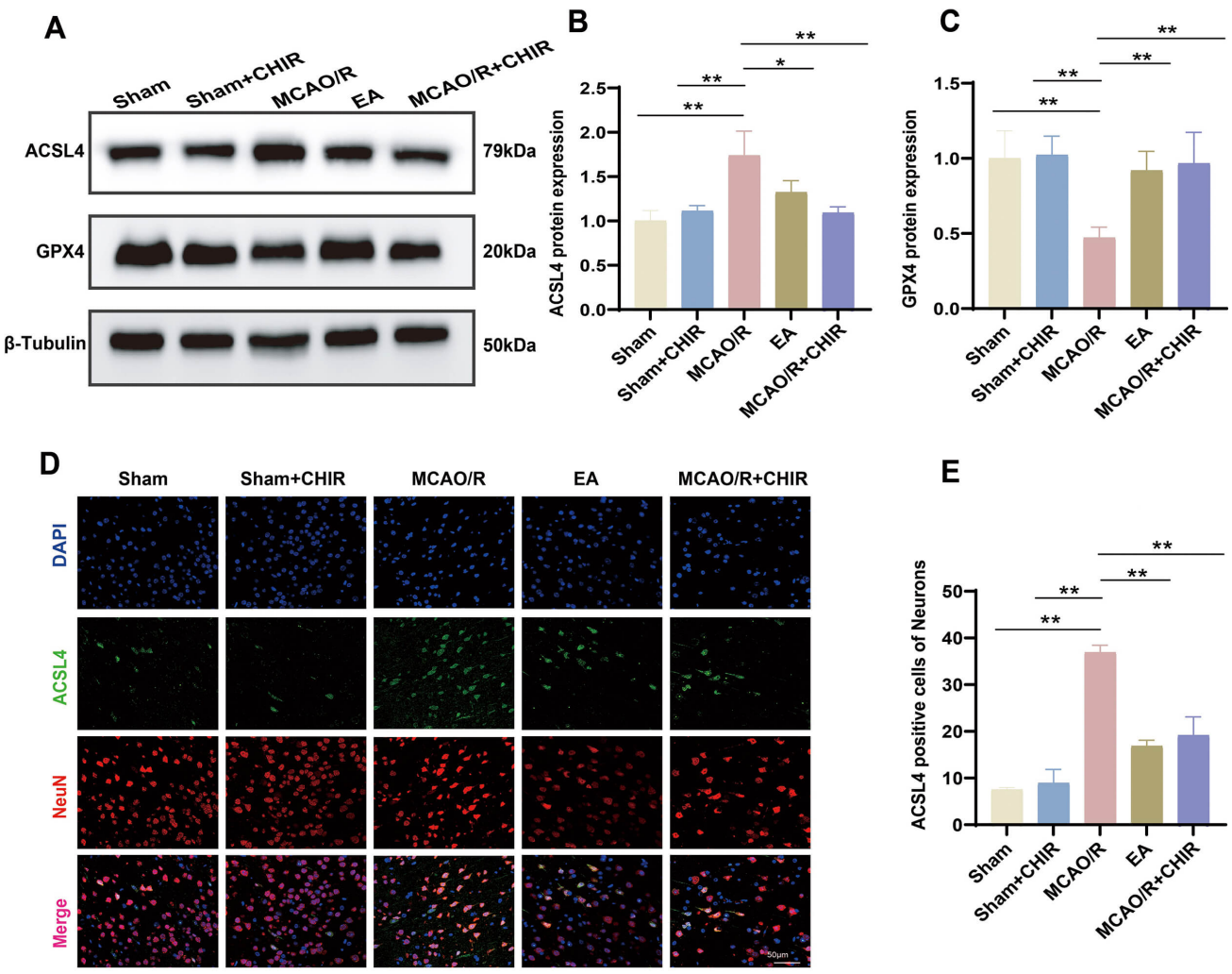


Fig. 5. EA modulates ACSL4/GPX4 expression and reduces neuronal ferroptosis-associated changes after MCAO/R. (A) Representative western blots of ACSL4 and GPX4. (B,C) Quantification of ACSL4 (B) and GPX4 (C) protein expression (n = 4). (D) NeuN/ACSL4 double immunofluorescence; nuclei are blue, ACSL4 is green, and NeuN is red. Scale bar = 50 μm. (E) Quantification of NeuN/ACSL4-colocalized positive cells (n = 3). Values are mean ± SD; *$p < 0.05$, **$p < 0.01$. NeuN, neuronal nuclear antigen.

CHIR increased NQO1 mRNA expression in Nrf2f/f + M/R mice ($p < 0.01$, Fig. 7B), but not in Nrf2f/N + M/R mice ($p > 0.05$). Western blotting showed that CHIR increased the p-GSK-3β/GSK-3β ratio in both genotypes (both $p < 0.05$), with no significant difference between genotypes after CHIR treatment ($p > 0.05$, Fig. 7C,D). CHIR also increased NQO1 protein expression in Nrf2f/f + M/R mice ($p < 0.01$), whereas the increase was not significant in Nrf2f/N + M/R mice ($p > 0.05$, Fig. 7C,E).

Further analysis showed that, in Nrf2f/f + M/R mice, CHIR increased SLC7A11 mRNA ($p < 0.01$), GPX4 mRNA ($p < 0.01$), SLC7A11 protein ($p < 0.05$), and GPX4 protein ($p < 0.01$, Fig. 7F–J). In Nrf2f/N + M/R mice, CHIR still increased SLC7A11 mRNA ($p < 0.01$, Fig. 7F), but the changes in GPX4 mRNA, SLC7A11 protein, and GPX4 protein were not significant (all $p > 0.05$, Fig. 7G,I,J).

Collectively, Nrf2 deficiency did not affect CHIR-mediated regulation of GSK-3β phosphorylation but markedly attenuated its downstream effects on NQO1, SLC7A11, and GPX4. These findings suggest that GSK-3β acts upstream of Nrf2 and that its anti-ferroptotic effects depend at least partly on Nrf2, further supporting the conclusion that EA inhibits MCAO/R-induced ferroptosis through the GSK-3β/NRF2 signaling axis.

4. Discussion

Overall, this study elucidated a molecular mechanism by which EA suppresses neuronal ferroptosis after MCAO/R through modulation of the GSK-3β/NRF2 signaling axis. We found that ischemia-reperfusion caused aberrant activation of GSK-3β, limited NRF2 protein stability and nuclear translocation, weakened endogenous antioxidant defenses, and further promoted Fe^{2+} accumulation, lipid peroxidation, and ferroptosis. EA inhibited GSK-3β activity, restored NRF2 expression and promoted its nu-

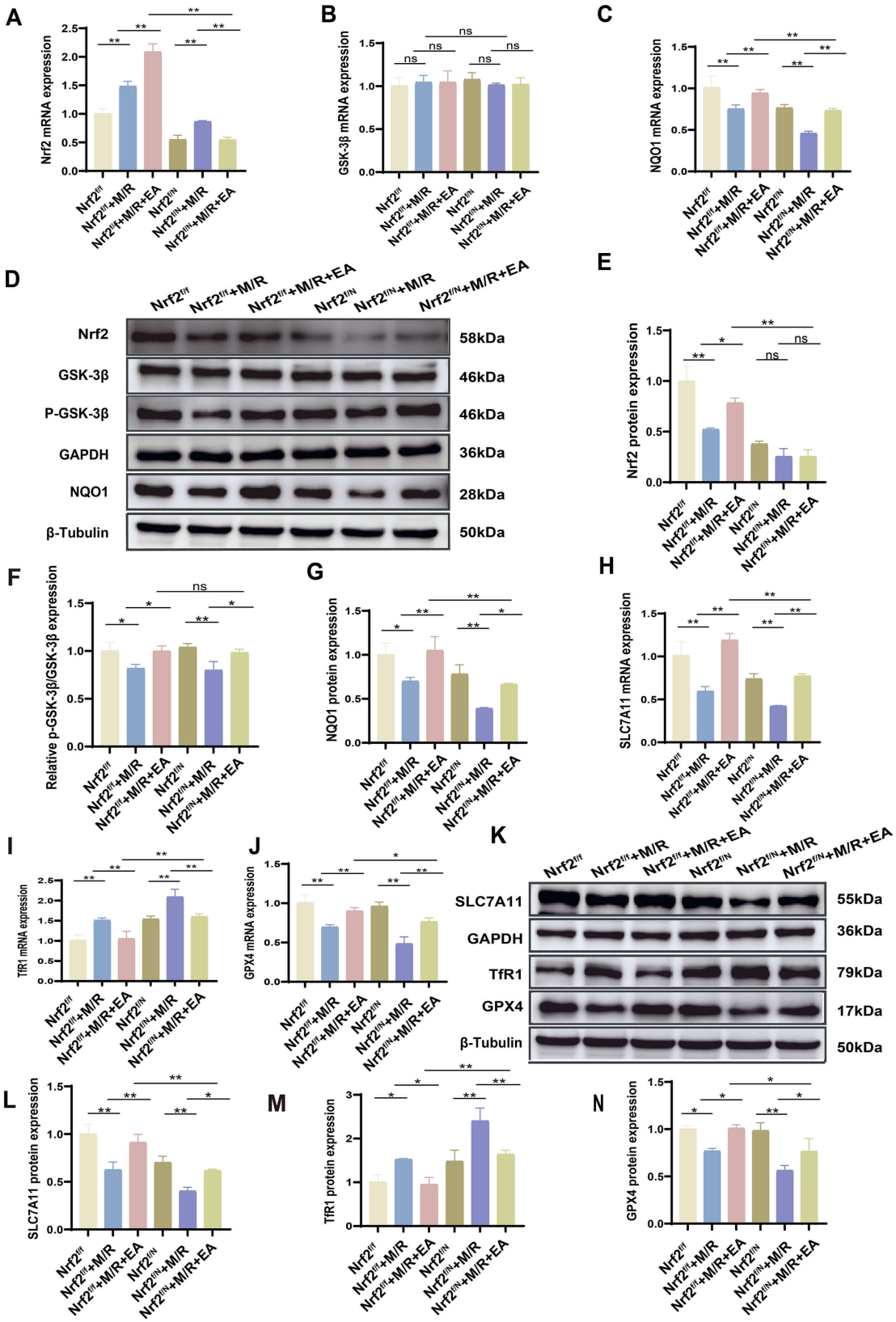


Fig. 6. Conditional Nrf2 deletion attenuates EA-mediated regulation of the GSK-3β/NRF2 pathway and ferroptosis-related molecules after MCAO/R. (A–C,H–J) RT-qPCR analysis of Nrf2 (A), GSK-3β (B), NQO1 (C), SLC7A11 (H), TfR1 (I), and GPX4 (J) mRNA expression (n = 5). (D,K) Representative western blots of NRF2, GSK-3β, p-GSK-3β, NQO1, SLC7A11, TfR1, and GPX4. (E–G,L–N) Quantification of NRF2 (E), the p-GSK-3β/GSK-3β ratio (F), NQO1 (G), SLC7A11 (L), TfR1 (M), and GPX4 (N) protein expression (n = 3). Values are mean ± SD; ns, not significant; *$p < 0.05$, **$p < 0.01$.

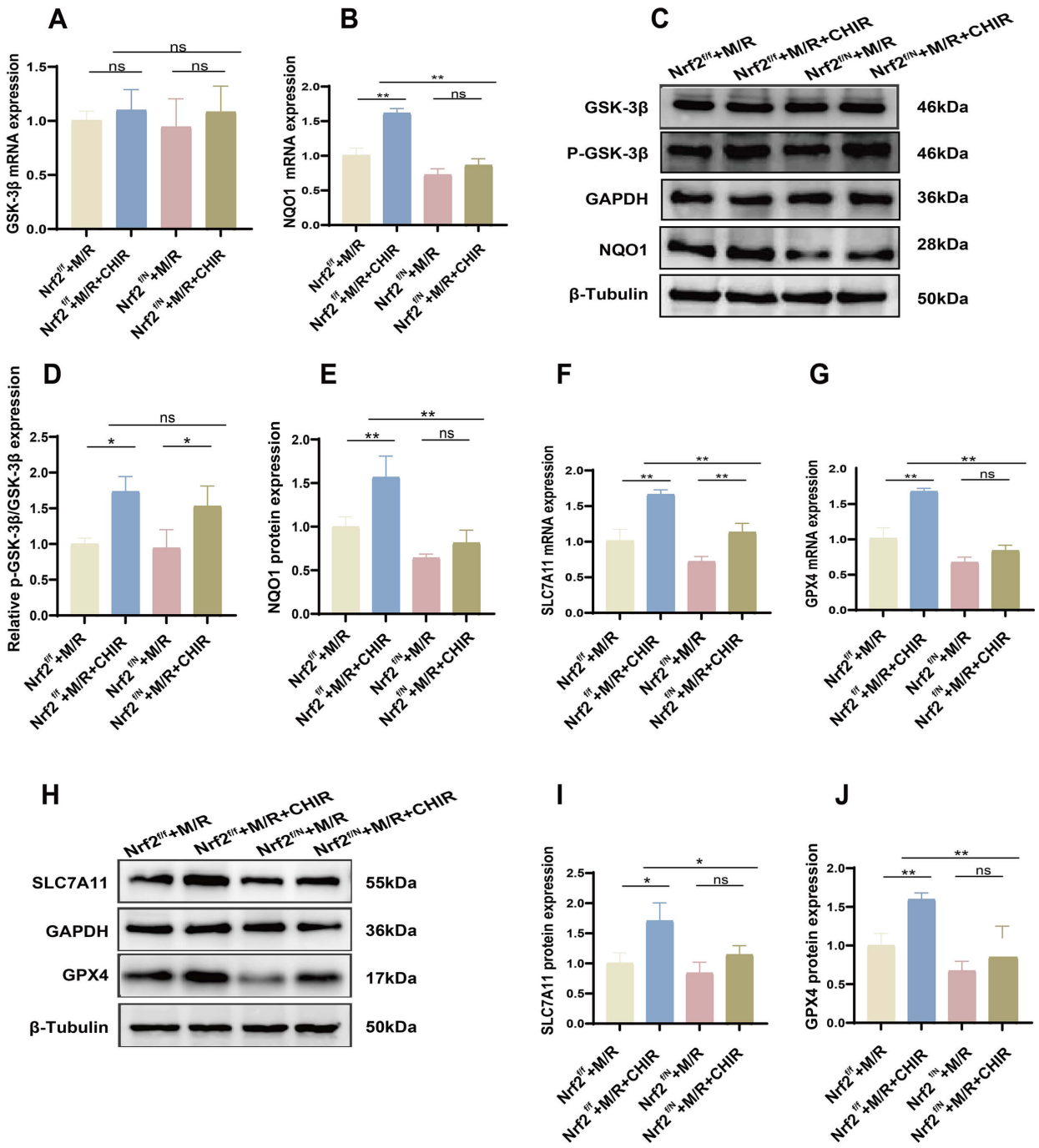


Fig. 7. Conditional Nrf2 deletion attenuates the downstream effects of GSK-3β inhibition after MCAO/R. (A,B,F,G) RT-qPCR analysis of GSK-3β (A), NQO1 (B), SLC7A11 (F), and GPX4 (G) mRNA expression (n = 5). (C,H) Representative western blots of GSK-3β, p-GSK-3β, NQO1, SLC7A11, and GPX4. (D,E,I,J) Quantification of the p-GSK-3β/GSK-3β ratio (D), NQO1 (E), SLC7A11 (I), and GPX4 (J) protein expression (n = 3). Values are mean ± SD; ns, not significant; *$p < 0.05$, **$p < 0.01$.

clear accumulation, increased the expression of antioxidant and anti-ferroptotic effectors including NQO1, SLC7A11, and GPX4, and reduced ACSL4 and TfR1 levels. Pharmacological inhibition of GSK-3β produced similar effects, whereas conditional Nrf2 knockout attenuated the protective effects of EA and the GSK-3β inhibitor. These pharmacological and genetic findings support GSK-3β as an upstream regulator of NRF2 and identify NRF2 as a key effector mediating the anti-ferroptotic effects of EA, suggesting that the GSK-3β/NRF2/ferroptosis axis may be an important mechanism underlying the beneficial effects of EA on ischemic brain injury.

NRF2 is an important transcription factor that maintains cellular redox homeostasis and exerts key protective effects during ischemic, inflammatory, and metabolic stress [18]. The classical view is that NRF2 is primarily reg-

ulated by Kelch-like ECH-associated protein 1 (KEAP1)-mediated degradation, through which continuous NRF2 degradation maintains low basal activity [19,20]. Recent studies have shown that GSK-3β can regulate NRF2 protein stability through a Neh6/β-transducin repeat-containing protein (β-TrCP)-dependent pathway, providing an additional layer of negative regulation distinct from the KEAP1 pathway [21,22]. In this study, Nrf2 mRNA expression increased after MCAO/R, whereas NRF2 protein levels decreased, suggesting that ischemia-induced oxidative stress activates the NRF2 transcriptional response but that impaired protein stability limits an effective antioxidant response. EA not only further increased Nrf2 mRNA expression but also restored NRF2 protein levels and promoted nuclear translocation, suggesting that it may enhance endogenous antioxidant defenses by improving functional activation of NRF2.

Previous studies have shown that EA ameliorates cerebral ischemic injury by suppressing oxidative stress [23], promoting angiogenesis [24], and reducing apoptosis [25]. The present study further demonstrated that EA improved neurological dysfunction, reduced cerebral infarct volume, and attenuated neuronal injury in MCAO/R mice. However, phenotypic improvement alone is insufficient to explain the underlying molecular basis. Because disruption of iron homeostasis, ROS accumulation, and lipid peroxidation are important drivers of post-ischemic ferroptosis, we further focused on neuronal ferroptosis and its upstream regulatory mechanisms.

GSK-3β is a serine/threonine protein kinase involved in the regulation of cell survival, oxidative stress, and cell death [26]. Previous studies have shown that aberrant GSK-3β activation promotes multiple forms of stress-related injury, whereas GSK-3β inhibition enhances cellular antioxidant capacity [27]. In NRF2 regulation, GSK-3β can limit NRF2 transcriptional activity by affecting its stability and subcellular localization [28]. We found that increased GSK-3β activity after MCAO/R was accompanied by reduced NRF2 protein levels, whereas GSK-3β inhibition restored NRF2 levels and promoted its nuclear accumulation; Co-IP further demonstrated a protein interaction between GSK-3β and NRF2. Together with previous evidence that GSK-3β regulates NRF2 nuclear translocation [13], these findings support GSK-3β as a potentially important regulatory node that suppresses NRF2 function under ischemia-reperfusion conditions.

To further clarify the causal relationship within this signaling axis, we used a conditional Nrf2-knockout model. When Nrf2 expression was intact, EA restored NQO1, SLC7A11, and GPX4 expression and suppressed abnormal changes in ferroptosis-related molecules such as TfR1; Nrf2 deficiency markedly attenuated these protective effects. At the same time, Nrf2 deficiency did not affect the regulation of GSK-3β activity by EA, indicating that GSK-3β acts upstream of NRF2. Similarly, the effect of CHIR-99021 on GSK-3β was independent of Nrf2, whereas its beneficial effects on downstream antioxidant molecules were markedly attenuated. These findings further establish the regulatory direction from GSK-3β to NRF2 and provide direct mechanistic evidence that EA suppresses ferroptosis through this pathway.

Notably, GSK-3β may link the GSK-3β/NRF2 axis identified in this study to our previous work on Wnt/β-catenin signaling. Our previous study showed that EA modulates the Wnt/β-catenin pathway and reduces GSK-3β expression [9]. Because GSK-3β participates in both β-catenin stability and NRF2 activity, it may serve as a common regulatory node connecting distinct protective signaling pathways. In addition, Wnt/β-catenin signaling is linked to the regulation of lipid metabolism [29]. GSK-3β may therefore coordinate redox and metabolic homeostasis under ischemic stress.

The present study further confirmed that EA modulates the GSK-3β/NRF2 signaling axis. EA inhibited GSK-3β activation, promoted NRF2 accumulation and nuclear translocation, and enhanced the downstream antioxidant response. These findings are consistent with previous reports of negative regulation of NRF2 by GSK-3β and EA-mediated enhancement of NRF2-related defense responses [8]. In addition, GSK-3β/NRF2 signaling has been implicated in ferroptosis regulation, and GSK-3β inhibition can promote NRF2 activation and attenuate ferroptosis [30,31]. Compared with previous studies, the present work combined pharmacological GSK-3β inhibition with conditional Nrf2 knockout to provide causal evidence supporting the key role of this signaling axis in the anti-ferroptotic effects of EA.

Ferroptosis is an iron-dependent form of regulated cell death characterized mainly by increased iron burden, enhanced lipid peroxidation, and abnormal ROS accumulation [32]. In this study, ferroptotic changes after MCAO/R were evaluated at multiple levels, including iron metabolism, redox status, and mitochondrial structure. MCAO/R increased Fe^{2+} and MDA levels, decreased SOD activity, GSH content, and the GSH/GSSG ratio, and was accompanied by mitochondrial ultrastructural damage; both EA and GSK-3β inhibition ameliorated these changes. Previous studies have shown that EA attenuates mitochondrial injury after cerebral ischemia [33]. The present findings further suggest that this protection may be related to correction of GSK-3β/NRF2 dysregulation and restoration of redox homeostasis.

GPX4 is a key enzyme in anti-ferroptotic defense that uses GSH to eliminate lipid hydroperoxides and thereby interrupt lipid peroxidation chain reactions [34]. Reduced GPX4 function leads to lipid-peroxide accumulation and promotes ferroptosis [35,36]. We found that MCAO/R decreased GPX4 and SLC7A11 expression, whereas EA, the GSK-3β inhibitor, and Fer-1 reversed these changes. Furthermore, Nrf2 deficiency attenuated the restoration of GPX4 by EA and GSK-3β inhibition, suggesting that the SLC7A11/GPX4 antioxidant system may be an important

effector arm of the anti-ferroptotic response mediated by the GSK-3β/NRF2 axis.

ACSL4 is an important lipid-metabolizing enzyme that promotes ferroptosis by increasing oxidizable lipid substrates through remodeling of polyunsaturated fatty acid-containing phospholipids [37]. Previous studies have shown that modulation of GPX4/ACSL4-related pathways can alleviate cerebral ischemia-reperfusion injury [38]. We found that MCAO/R increased ACSL4 and decreased GPX4, whereas both EA and GSK-3β inhibition reversed these changes. NeuN/ACSL4 double-labeling further showed that EA reduced abnormal neuronal ACSL4 expression, providing additional evidence that GSK-3β/NRF2 signaling not only affects overall oxidative status but is also involved in neuronal ferroptosis.

In summary, this study revealed a mechanism by which EA suppresses neuronal ferroptosis after MCAO/R through the GSK-3β/NRF2 signaling axis. Ischemia-reperfusion induced aberrant GSK-3β activation, resulting in reduced NRF2 stability and insufficient antioxidant defense, which further promoted iron accumulation, lipid peroxidation, and ferroptosis. By inhibiting GSK-3β, restoring NRF2 function, and activating downstream defense systems including NQO1, SLC7A11, and GPX4, EA attenuated neuronal ferroptotic injury. Through the combined use of pharmacological inhibition, protein-interaction analysis, and genetic validation, this study further clarified the regulatory relationship between GSK-3β and NRF2 and suggests that the GSK-3β/NRF2/ferroptosis axis may represent an important target for intervention in ischemic brain injury.

5. Limitations

This study has several limitations. First, the placement of GSK-3β upstream of NRF2 is supported by CHIR-99021 treatment, Co-IP, and the persistence of EA- and CHIR-induced changes in GSK-3β phosphorylation after Nrf2 deletion. However, GSK-3β was not genetically manipulated, and Co-IP demonstrates association rather than direct phosphorylation of NRF2. NRF2 phosphorylation, ubiquitination, and proteasomal degradation were also not measured, and an EA + CHIR combination group was not included to test pathway occlusion or additivity. Thus, the data support the GSK-3β/NRF2 regulatory relationship but do not define the complete molecular sequence by which EA stabilizes and activates NRF2.

Second, the conditional Nrf2 model was generated using Nestin-Cre, whereas most molecular measurements were performed in bulk ipsilateral ischemic cortical tissue. Although NeuN/ACSL4 double immunofluorescence supports a neuronal component of the ferroptosis-related changes, the present design cannot assign all changes in NRF2 signaling or downstream ferroptosis-related proteins specifically to mature neurons or exclude contributions from other neural cell populations.

Third, the Fer-1 experiment was used as a pharmacological reference for ferroptosis and included five animals in the final analysis, with Fer-1 comparisons focused on the molecular endpoints shown in Fig. 3. Fer-1 was not evaluated across the neurological, infarct, mitochondrial, and redox outcomes used for EA and CHIR. In addition, ferroptosis was inferred from convergent biochemical, protein, immunofluorescence, and ultrastructural evidence rather than direct measurement of oxidized phospholipid species. Therefore, the contribution of ferroptosis to the functional neuroprotection produced by EA cannot be quantified from the present data.

Fourth, all experimental mice included in the study were male, EA was tested using a single acupoint combination and stimulation regimen, and the principal outcome assessment was performed within 7 days after MCAO/R. Several molecular and histological endpoints also used relatively small group sizes (n = 3–5). Consequently, sex-dependent effects, the dose-response and therapeutic window of EA, and the durability of the observed neuroprotection beyond the early/subacute period remain unresolved.

6. Conclusions

In summary, we demonstrated that electroacupuncture can markedly promote the recovery of CIRI. We further revealed the interaction between GSK-3β and NRF2, meanwhile, we found that the GSK-3β/NRF2 signaling pathway plays a key role in the electroacupuncture-mediated inhibition of ferroptosis. These findings suggest that the pharmacological inhibition of GSK-3β could be a novel treatment method for IS.

Availability of Data and Materials

The data utilized to bolster the results of this research are incorporated within the article.

Author Contributions

YSH contributed to the conception and design of the study and supervised the research. WXX and RZ contributed equally to this work. WXX and RZ jointly designed and performed the experiments, and RZ interpreted the data and wrote the manuscript. XXL, CCX, JJD, SJL, and YX analyzed the data. All authors critically reviewed and revised the academic content of the manuscript. All authors read and approved the final manuscript. All authors have participated sufficiently in the work and agreed to be accountable for all aspects of the work.

Ethics Approval and Consent to Participate

All experimental procedures were approved by the Animal Ethics Committee of the Anhui University of Chinese Medicine (approval number: AHUCM-mouse-2023131) and were carried out following the guidelines of the China Animal Care Committee. The study was carried out in accordance with the ARRIVE guidelines.

Acknowledgment

We are very grateful for the graphical support provided by FigDraw.

Funding

This study was supported by the National Natural Science Foundation of China (No. 82274656, 82575236). Research Funds of Center for Xin'an Medicine and Modernization of Traditional Chinese Medicine of IHM (2023CXMMTCM002). Supported by Program for Excellent Sci-tech Innovation Teams of Anhui Provincial Department of Education-2025AHGXZK10040.

Conflicts of Interest

The authors declare no conflicts of interest.

Supplementary Material

Supplementary material associated with this article can be found, in the online version, at https://doi.org/10.31083/JIN53689.

References

[1] Walter K. What Is Acute Ischemic Stroke? JAMA. 2022; 327: 885. https://doi.org/10.1001/jama.2022.1420

[2] Khoshnam SE, Winlow W, Farzaneh M, Farbood Y, Moghaddam HF. Pathogenic mechanisms following ischemic stroke. Neurological Sciences : Official Journal of the Italian Neurological Society and of the Italian Society of Clinical Neurophysiology. 2017; 38: 1167–1186. https://doi.org/10.1007/s10072-017-2938-1

[3] Yang C, Hawkins KE, Doré S, Candelario-Jalil E. Neuroinflammatory mechanisms of blood-brain barrier damage in ischemic stroke. American Journal of Physiology. Cell Physiology. 2019; 316: C135–C153. https://doi.org/10.1152/ajpcell.00136.2018

[4] Dodson M, Castro-Portuguez R, Zhang DD. NRF2 plays a critical role in mitigating lipid peroxidation and ferroptosis. Redox Biology. 2019; 23: 101107. https://doi.org/10.1016/j.redox.2019.101107

[5] Wang R, Xu JF. AMPK mediates the anti-ferroptosis effect of acupuncture in cerebral ischemia-reperfusion rats. Brain Research. 2025; 1860: 149662. https://doi.org/10.1016/j.brainres.2025.149662

[6] Zhang W, Han L, Wen Y, Su L, Li Y, Luo X. Electroacupuncture reverses endothelial cell death and promotes angiogenesis through the VEGF/Notch signaling pathway after focal cerebral ischemia-reperfusion injury. Brain and Behavior. 2023; 13: e2912. https://doi.org/10.1002/brb3.2912

[7] Xing Y, Zhang M, Wang MM, Feng YS, Dong F, Zhang F. The Anti-apoptosis Effect of Single Electroacupuncture Treatment *via* Suppressing Neuronal Autophagy in the Acute Stage of Ischemic Stroke Without Infarct Alleviation. Frontiers in Cellular Neuroscience. 2021; 15: 633280. https://doi.org/10.3389/fncel.2021.633280

[8] Ni C, Huang B, Huang Y, Wen Z, Luo S. Keap1-independent GSK-3β/Nrf2 signaling mediates electroacupuncture inhibition of oxidative stress to induce cerebral ischemia-reperfusion tolerance. Brain Research Bulletin. 2024; 217: 111071. https://doi.org/10.1016/j.brainresbull.2024.111071

[9] Li GD, Li XX, Dong JJ, Wu Y, Han YS. Effect of electroacupuncture on neurovascular unit and Wnt/β-catenin signaling in rats with cerebral ischemia. Zhen Ci Yan Jiu = Acupuncture Research. 2021; 46: 87–94. https://doi.org/10.13702/j.1000-0607.200819 (In Chinese)

[10] Li G, Li X, Dong J, Han Y. Electroacupuncture Ameliorates Cerebral Ischemic Injury by Inhibiting Ferroptosis. Frontiers in Neurology. 2021; 12: 619043. https://doi.org/10.3389/fneur.2021.619043

[11] Zhu W, Dong J, Han Y. Electroacupuncture Downregulating Neuronal Ferroptosis in MCAO/R Rats by Activating Nrf2/SLC7A11/GPX4 Axis. Neurochemical Research. 2024; 49: 2105–2119. https://doi.org/10.1007/s11064-024-04185-x

[12] Russell JC, Kishimoto K, O'Driscoll C, Hossain MA. Neuronal pentraxin 1 induction in hypoxic-ischemic neuronal death is regulated via a glycogen synthase kinase-3α/β dependent mechanism. Cellular Signalling. 2011; 23: 673–682. https://doi.org/10.1016/j.cellsig.2010.11.021

[13] Chen X, Liu Y, Zhu J, Lei S, Dong Y, Li L, et al. GSK-3β downregulates Nrf2 in cultured cortical neurons and in a rat model of cerebral ischemia-reperfusion. Scientific Reports. 2016; 6: 20196. https://doi.org/10.1038/srep20196

[14] Wu X, Liu C, Li Z, Gai C, Ding D, Chen W, et al. Regulation of GSK3β/Nrf2 signaling pathway modulated erastin-induced ferroptosis in breast cancer. Molecular and Cellular Biochemistry. 2020; 473: 217–228. https://doi.org/10.1007/s11010-020-03821-8

[15] Longa EZ, Weinstein PR, Carlson S, Cummins R. Reversible middle cerebral artery occlusion without craniectomy in rats. Stroke. 1989; 20: 84–91. https://doi.org/10.1161/01.str.20.1.84

[16] Chinese Association of Acupuncture-Moxibustion. Nomenclature and location of acupuncture points commonly used in laboratory animals—Part 3: Mice. Acupuncture Research. 2021; 46: 445-446. https://www.zhenciyanjiu.cn/en/article/40641863/

[17] Paxinos G, Franklin KBJ. Paxinos and Franklin's The Mouse Brain in Stereotaxic Coordinates. 4th edn. Academic Press: Amsterdam. 2013.

[18] Hayes JD, Dayalan Naidu S, Dinkova-Kostova AT. Regulating Nrf2 activity: ubiquitin ligases and signaling molecules in redox homeostasis. Trends in Biochemical Sciences. 2025; 50: 179–205. https://doi.org/10.1016/j.tibs.2024.12.010

[19] Baird L, Yamamoto M. The Molecular Mechanisms Regulating the KEAP1-NRF2 Pathway. Molecular and Cellular Biology. 2020; 40: e00099–20. https://doi.org/10.1128/MCB.00099-20

[20] Attri M, Kuwar OK. The KEAP1-Cullin3-RBX1-Nrf2 Axis in Redox Homeostasis: Molecular Mechanisms, Pathophysiological Roles, and Precision Therapeutic Opportunities. Molecular Neurobiology. 2025; 63: 15. https://doi.org/10.1007/s12035-025-05313-6

[21] Rada P, Rojo AI, Evrard-Todeschi N, Innamorato NG, Cotte A, Jaworski T, et al. Structural and functional characterization of Nrf2 degradation by the glycogen synthase kinase 3/β-TrCP axis. Molecular and Cellular Biology. 2012; 32: 3486–3499. https://doi.org/10.1128/MCB.00180-12

[22] Chowdhry S, Zhang Y, McMahon M, Sutherland C, Cuadrado A, Hayes JD. Nrf2 is controlled by two distinct β-TrCP recognition motifs in its Neh6 domain, one of which can be modulated by GSK-3 activity. Oncogene. 2013; 32: 3765–3781. https://doi.org/10.1038/onc.2012.388

[23] Li N, Guo Y, Gong Y, Zhang Y, Fan W, Yao K, et al. The Anti-Inflammatory Actions and Mechanisms of Acupuncture from Acupoint to Target Organs via Neuro-Immune Regulation. Journal of Inflammation Research. 2021; 14: 7191–7224. https://doi.org/10.2147/JIR.S341581

[24] Xu SY, Zeng CL, Ni SM, Peng YJ. The Angiogenesis Effects of Electro-acupuncture Treatment via Exosomal miR-210 in Cerebral Ischemia-Reperfusion Rats. Current Neurovascular Research. 2022; 19: 61–72. https://doi.org/10.2174/1567202619666220321115412

[25] Xue X, You Y, Tao J, Ye X, Huang J, Yang S, et al. Electro-

acupuncture at points of Zusanli and Quchi exerts anti-apoptotic effect through the modulation of PI3K/Akt signaling pathway. Neuroscience Letters. 2014; 558: 14–19. https://doi.org/10.1016/j.neulet.2013.10.029

[26] Kaidanovich-Beilin O, Woodgett JR. GSK-3: Functional Insights from Cell Biology and Animal Models. Frontiers in Molecular Neuroscience. 2011; 4: 40. https://doi.org/10.3389/fnmol.2011.00040

[27] Rojo AI, Sagarra MRD, Cuadrado A. GSK-3beta downregulates the transcription factor Nrf2 after oxidant damage: relevance to exposure of neuronal cells to oxidative stress. Journal of Neurochemistry. 2008; 105: 192–202. https://doi.org/10.1111/j.1471-4159.2007.05124.x

[28] Jain AK, Jaiswal AK. GSK-3beta acts upstream of Fyn kinase in regulation of nuclear export and degradation of NF-E2 related factor 2. The Journal of Biological Chemistry. 2007; 282: 16502–16510. https://doi.org/10.1074/jbc.M611336200

[29] Bagchi DP, Nishii A, Li Z, DelProposto JB, Corsa CA, Mori H, et al. Wnt/β-catenin signaling regulates adipose tissue lipogenesis and adipocyte-specific loss is rigorously defended by neighboring stromal-vascular cells. Molecular Metabolism. 2020; 42: 101078. https://doi.org/10.1016/j.molmet.2020.101078

[30] Xu F, Zhang J, Ji L, Cui W, Cui J, Tang Z, et al. Inhibition of Non-small Cell Lung Cancer by Ferroptosis and Apoptosis Induction through P53 and GSK-3β/Nrf2 Signal Pathways using Qingrehuoxue Formula. Journal of Cancer. 2023; 14: 336–349. https://doi.org/10.7150/jca.79465

[31] Tang Z, Chen K, Sun C, Ying X, Li M. Cordycepin inhibits kidney injury by regulating GSK-3β-mediated Nrf2 activation. Journal of Biochemical and Molecular Toxicology. 2024; 38: e23600. https://doi.org/10.1002/jbt.23600

[32] Li J, Cao F, Yin HL, Huang ZJ, Lin ZT, Mao N, et al. Ferroptosis: past, present and future. Cell Death & Disease. 2020; 11: 88. https://doi.org/10.1038/s41419-020-2298-2

[33] Wang H, Chen S, Zhang Y, Xu H, Sun H. Electroacupuncture ameliorates neuronal injury by Pink1/Parkin-mediated mitophagy clearance in cerebral ischemia-reperfusion. Nitric Oxide : Biology and Chemistry. 2019; 91: 23–34. https://doi.org/10.1016/j.niox.2019.07.004

[34] Lana JV, Rios A, Takeyama R, Santos N, Pires L, Santos GS, et al. Nebulized Glutathione as a Key Antioxidant for the Treatment of Oxidative Stress in Neurodegenerative Conditions. Nutrients. 2024; 16: 2476. https://doi.org/10.3390/nu16152476

[35] Zhang Q, Jia M, Wang Y, Wang Q, Wu J. Cell Death Mechanisms in Cerebral Ischemia-Reperfusion Injury. Neurochemical Research. 2022; 47: 3525–3542. https://doi.org/10.1007/s11064-022-03697-8

[36] Tuo QZ, Lei P. Ferroptosis in ischemic stroke: Animal models and mechanisms. Zoological Research. 2024; 45: 1235–1248. https://doi.org/10.24272/j.issn.2095-8137.2024.239

[37] Zhuo B, Qin C, Deng S, Jiang H, Si S, Tao F, et al. The role of ACSL4 in stroke: mechanisms and potential therapeutic target. Molecular and Cellular Biochemistry. 2025; 480: 2223–2246. https://doi.org/10.1007/s11010-024-05150-6

[38] Li M, Meng Z, Yu S, Li J, Wang Y, Yang W, et al. Baicalein ameliorates cerebral ischemia-reperfusion injury by inhibiting ferroptosis via regulating GPX4/ACSL4/ACSL3 axis. Chemico-biological Interactions. 2022; 366: 110137. https://doi.org/10.1016/j.cbi.2022.110137